Deformation Mechanisms of Offshore Monopile Foundations Accounting for Cyclic Mobility Effects

Barari, Amin; Bagheri, Mohsen; Rouainia, Mohamed; Ibsen, Lars Bo

Published in:
Soil Dynamics and Earthquake Engineering

DOI (link to publication from Publisher):
10.1016/j.soildyn.2017.03.008

Publication date:
2017

Document Version
Accepted author manuscript, peer reviewed version

Contents lists available at ScienceDirect

Soil Dynamics and Earthquake Engineering

journal homepage: www.elsevier.com

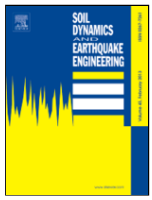

Deformation mechanisms for offshore monopile foundations accounting for cyclic mobility effects

A. Barari [a, b, *], M. Bagheri [c], M. Rouainia [d], L.B. Ibsen [a]

[a] Department of Civil Engineering, Aalborg University, Thomas Manns Vej 23, Aalborg Ø, 9220 Aalborg, Denmark
[b] Department of Civil and Environmental Engineering, Virginia Tech, Blacksburg, VA 24061, USA
[c] Department of Civil Engineering, Babol University of Technology, Babol, Iran
[d] School of Civil Engineering and Geosciences, Newcastle University, Newcastle upon Tyne NE1 7RU, UK

ARTICLE INFO

Keywords:
Wind turbine foundation
Long-term cyclic loading
Dense sand
Cyclic mobility
Transient

ABSTRACT

There has been a huge surge in the construction of marine facilities (e.g., wind turbines) in Europe, despite the many unknowns regarding their long-term performance. This paper presents a new framework for design strategy based on performance measures for cyclic horizontally loaded monopile foundations located in saturated and dry dense sand, by considering pile deformations and pore pressure accumulation effects. A three-dimensional finite element model was developed to investigate the behavior of large-diameter piles. The model accounts for nonlinear dynamic interactions in offshore platforms under harsh combined moment and horizontal environmental loads, with emphasis on the cyclic mobility of the surrounding cohesionless subsoil and associated shear.

The maximum moment applied in the cyclic analyses is varied from 18% to 47% of the ultimate resistance. The considered data reflect behavior at the expected load amplitudes and cycle numbers during the service life of operation.

For low numbers of load cycles (<1000 cycles), there were no differences between the power law and logarithmic approaches in terms of describing the accumulated deformations; however, for high numbers of cycles (<10,000 cycles), the logarithmic law was less suited to describe the accumulation response. Magnitude of cyclic loads was found to cause a linear increase in the accumulated rotation. The results from short-term and long-term dynamic response of monopiles indicate that few load cycles with higher load levels are the main concerns in accumulation of pile rotation rather than thousands of load cycles with low amplitudes.

1. Introduction

The design and analysis of foundations for offshore turbines are challenging endeavors, due to the harsh environmental conditions that these structures experience. Recently, such structures have been developed extensively in Europe (e.g., see [27,2,4–7,29,22,23,24,9,15,28]). Foundation concepts that are frequently used for offshore wind turbines include monopiles, jackets, and tension-leg floating substructures. [15] described a state-of-the-art in foundation design for offshore platforms. Under suitable soil conditions, monopiles have shown to be feasible in water depths of up to 35 m.

Due to their slender nature, offshore wind turbines are dynamically sensitive when used under adverse environmental conditions. During the lifetime of a wind turbine, a monopile foundation may be subjected to either a small number of lateral load cycles with large amplitudes, as a result of severe earthquakes or storms, or to regular of lateral load cycles with intermediate amplitudes, due to wave loading in the fatigue and serviceability limit states (FLS and SLS, respectively) [44,50]. In the literature, analytical approaches (e.g., subgrade reaction methods) and finite-element (FE) techniques have been widely used to determine the response of offshore piles to lateral loading.

The p-y curve is a subgrade reaction technique derived from large-scale testing on two flexible, slender piles, according to the design standards [3] and [13]. Both standards recommend the p-y curves initially formulated by [41] and [36]. The p-y methodology is not based on rational mechanics, and material parameters are typically chosen empirically, through observations of pile behavior. Several factors (e.g., diameter and soil-pile stiffness) are not addressed in this methodology,

* Corresponding author at: Department of Civil Engineering, Aalborg University, Thomas Manns Vej 23, Aalborg Ø, 9220 Aalborg, Denmark.
Email address: abarari@vt.edu (A. Barari)

http://dx.doi.org/10.1016/j.soildyn.2017.03.008
Received 22 October 2014; Received in revised form 19 February 2017; Accepted 9 March 2017
Available online xxx
0267-7261/

which can lead to severe restrictions. Applying design standards for stiff offshore piles to wind turbines with a slenderness ratio less than 10 is not within the verified range of these standards.

Many authors have provided long-term performance predictions and observations for monopiles. [31] was among the first to address the issue of accumulated rotation and stiffness changes for small-scale stiff piles after long-term cyclic loading between 8000 and 60,000 load cycles. They thoroughly investigated the dependence of accumulated rotation on relative density, which they found to be very sensitive to cyclic load characteristics. [49] developed and implemented a fully coupled, two-phase, three-dimensional (3D) FE model for explicitly describing the accumulation of water pressure close to the monopile as a function of the number of cycles. [26] and [11] described the change in the bedding resistance in subgrade reaction methods with the number of load cycles.

1.1. Aim and scope of the paper

Although several authors have performed small-scale 1-g tests [31,39,40,44], the applicability of the proposed observations to the design of full-scale monopiles remains questionable. In particular, the stress distribution in a 1-g experiment is not identical to that in the full-scale condition. On the other hand, although values can be scaled in centrifuge experiments conducted at Ng and at the correct stress level corresponding to the full-scale prototype, scaling to prototype is still a difficult task, especially for cyclic tests and limitations exist [26].

This article describes a numerical model for predicting the accumulated pile rotation under one-way cyclic and transient lateral loading, as well as applications to investigate stress paths and soil-pile interactions. The full-scale numerical simulations reported in this paper offer promising predictions for the salient features of soil behavior that were previously not accounted for offshore monopiles. This paper complements previous studies in the field by presenting a series of parametric studies of the developed model predictions.

2. Dynamic considerations of offshore wind turbines

A wind turbine tower is influenced by two types of loading [33]. The *blade-passing effect* is the cyclic loading (i.e., 2p or 3p for a two- or three-bladed wind turbine) exerted by the blades on the upper side of the tower. *Wind loading* refers to a relatively constant load exerted by the wind on the lower side of the tower. The cyclic behavior of the soil-pile system can be evaluated according to the accumulated rotation and the stiffness of the entire system needed to maintain its efficiency. The wind turbine supplier usually specifies a constant limit for the pile rotation, typically around 0.5° [27].

The first modal frequency of a wind turbine will be within the range of 0.01–1 Hz making it relevant to the discussion of offshore wind turbines [8]. Typically, the peak frequencies of extreme waves and energy-rich wind turbulence are around 0.07–0.14 Hz and 0.1 Hz, respectively. To avoid system resonance, monopile foundations for offshore wind turbines are designed such that the first natural frequency lies outside the regions of the rotor frequency, 1 P (0.17–0.33 Hz), and the blade passing frequency, 3 P (0.5–1 Hz). Fig. 1 shows the main frequencies for a typical three-bladed wind turbine. The rotation and stiffness are the primary drivers in the design of offshore wind turbines, with the SLS and FLS being the primary loading states for design.

The desired frequency for a fixed wind turbine lies in the "Soft-Stiff" region between the turbine and blade-passing frequencies, wherein the support structure shows higher flexibility, reducing the material costs [8]. Typically, the region before 1 P, which contains the wave and wind excitation frequencies, is called the "Soft-Soft" region; the region after 3 P in which the natural frequency is higher than both

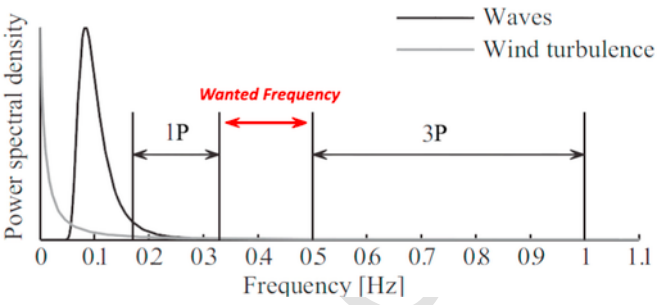

Fig. 1. Frequencies distribution for a fully operational Vestas 4.5 MW wind turbine [30].

driving frequencies is known as the "Stiff-Stiff" region. The global system is too flexible in the Soft-Soft region, but too rigid in the Stiff-Stiff region, making these regions unsuitable for design [19].

In offshore practice and presumed in the present study, frequency effects for dry sand seem to be negligible in loading frequencies below 1 Hz [18,51]. In the presence of water, the sand permeability and drainage conditions play important roles in terms of how the loading rate influences the cyclic behavior; this influence is mainly due to the accumulation of pore water pressure (PWP) with every cycle, which shall be discussed in subsequent sections.

3. Problem definition and methodology

3.1. System analyzed and FE model

A study was performed on a non-slender pile under different loading conditions. A 3D nonlinear static-dynamic model of a soil-pile system was developed in the FE code OpenSees version 1.7.3 [34]. A total of 384 elements were employed. Soil and pile elements were modeled by using 8-node, fully coupled (solid-fluid) brick and beam elements with 4 and 6 degrees of freedom (DOFs), respectively. Rigid beam-column connections, normal to the pile longitudinal axis, were used to represent the geometric space occupied by the pile. The 3D brick elements of the soil domain were connected to the pile geometric configuration at the outer nodes of the rigid links, this was achieved by equal DOF constraint in OpenSees for translations only. Three-dimensional modeling relies on the use of a validated fully coupled porous media (soil skeleton)-pore fluid (water) dynamic FE formulation. No special elements were defined for the soil-pile interface as the soil constitutive model accounts for the interface interaction [20].

Fig. 2 depicts a typical FE discretisation, together with the detailed loading scenarios applied to the FE models (length = 100 m, depth = 45 m). The generated model can be visualized using GID software [14]. A monopile diameter of 7.5 m with varying embedded length and wall thickness of 9 cm was assumed. In the numerical simulations, the pipe section of the monopile was replaced by a solid section with equivalent bending stiffness. The suitability of this simplification was previously confirmed by [1,4]. The bottom boundary of the model was taken to be 15 m below the base of the monopile. When a model length of 100 m was used, the calculated behavior of the monopile was not influenced by the boundaries. Table 1 provides the characteristics of the model parameters for the physical pile structure.

To improve the computational efficiency, only half of the piles were discretised. To represent the bedrock layer, all DOFs were restrained at the bottom boundary of the meshes. All symmetry planes were fixed against displacement normal to the symmetry faces, but were free to move on the surface of the plane. All simulations were undertaken using the OpenSees based on a u-p formulation. The Inelastic soil behavior was described by a multi-surface yield surface with nonlinear kinematic hardening and an associated plastic flow rule.

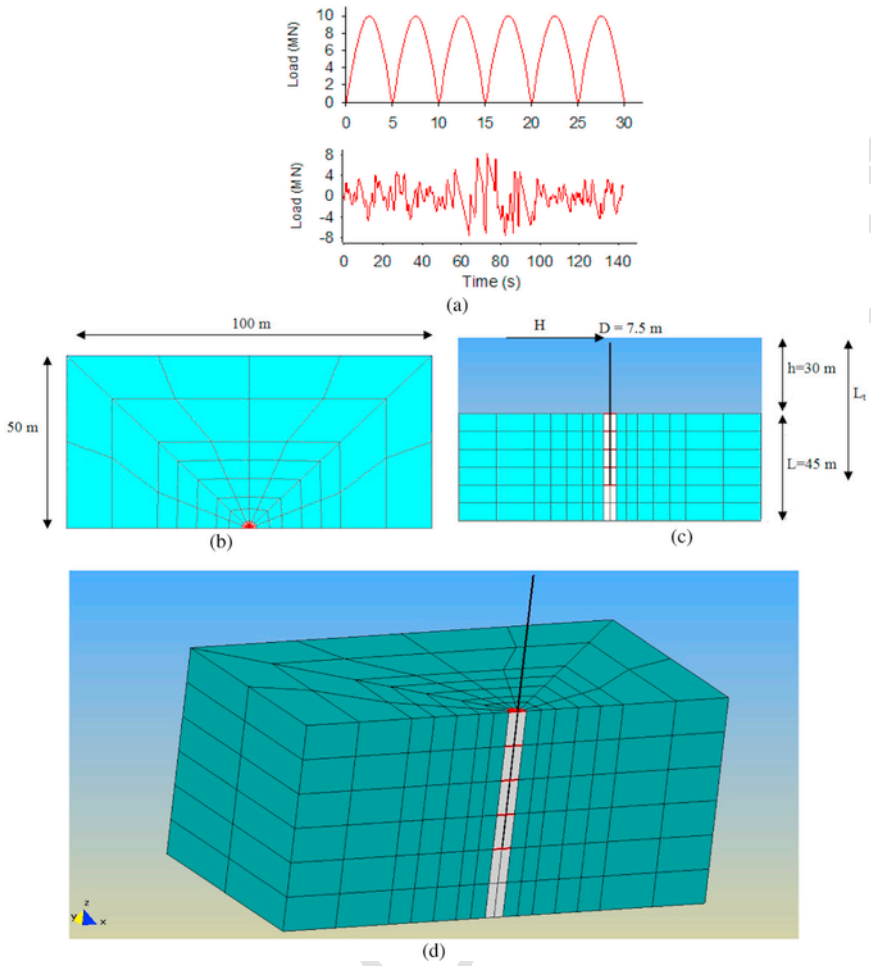

Fig. 2. Typical FE mesh of the developed numerical model: schematic illustration in dense sand subjected to the one-way and transient loading: (a) typical load time histories showing sinusoidal loading and an extreme event (b) plan view (c) side view (d) three dimensional view of Finite Element mesh.

Table 1
Pile characteristics.

Parameters	Symbol	Values
Total length	L_t	20, 30, 40, 60 m
Embedded depth	L	20, 30 m
Outer diameter	D	7.5 m
Pile wall thickness	t_p	0.09 m
Equivalent diameter	D_e	4.1 m
Young's modulus	E	2.1×10^8 kPa
Moment of inertia Young's modulus	I	14.84 m^4
Bending stiffness	EI	3.12×10^9 kN m^2

Three cases of static and dynamic loading, at the head of the pile, were considered. Each case was subdivided into different loading paths and soil characteristics:

- Case A: Cyclic loading on a pile with a diameter of 0.72 m, wall thickness of 0.06 m, and subjected to (i) 12 cycles from 960 up to 480 kN (P32) and (ii) 12 cycles from 960 kN up to 0 kN (P344);
- Case B: Static pushover-type of analysis on a hollow steel monopile of 7.5 m in diameter;
- Case C: Dynamic loading on large-diameter monopile, with (i) 1000 cycles of 0.2 Hz one-way cyclic lateral loads of 7.2, 10 and18.8 MN for dry sand; (ii) 500 cycles of 0.2 Hz one-way cyclic lateral loads of 7.2 and 10 MN for saturated sand; and (iii) transient effects due to a typical storm combined with cyclic loading.

3.2. Soil constitutive modeling

This paper presents a brief overview of the equations used to generate the nonlinear soil model for predicting the cyclic behavior of granular materials and pile responses.

The multisurface-plasticity theory for frictional cohesionless soils described by [53] was employed to simulate the nonlinear shear behavior of dense sand next to the foundation. The model uses a purely deviatoric kinematic hardening rule [38] with flow rules allowing for representing the hysteretic cyclic shear stress-strain response of the soil. The new flow rules implemented by [16] in OpenSees change the essentials of the original framework [38] in order to incorporate the cyclic mobility mechanisms.

The model was used to distinguish the nonlinear response as a function of the soil stiffness, permeability, and dilation potential. It accounted for time-varying strength changes, based on estimates of the pore-pressure field adjacent to the pile, and simulated the rate-dependency of the response due to different loading conditions.

If P denotes the direction of plastic flow, the level of dilation or contraction during cyclic loading is defined by a volumetric component P'' as:

$$P'' = \begin{Bmatrix} \frac{1-(\eta/\eta_{PT})^2}{1+(\eta/\eta_{PT})^2} c_1 \quad (for\ contraction) \\ \frac{1-(\eta/\eta_{PT})^2}{1+(\eta/\eta_{PT})^2} d_1 \exp\left(d_2 \gamma_d\right) \quad (for\ dilation) \end{Bmatrix} \tag{1}$$

where c_1, d_1, and d_2 are coefficients modeling the amount of plastic shear work done when the soil is in contraction (c_1) and dilation (d_1, d_2). Octahedral shear strain and stress ratio are modeled by γ_d and η respectively as introduced by [52]. The stress ratio of the Phase Transformation (PT) surface [25] is also defined by η_{PT}. Please note that if $\left(1-(\eta/\eta_{PT})^2\right)$ is positive, the stress states lies below the PT surface. On the other hand, a negative value implies that the stress state lies above the PT surface.

3.3. Comparison with results of centrifuge modeling

The well-documented centrifuge test of [42] on a pile founded on dense sand exposed to a cyclic horizontal load was modeled numerically (Case A). One- way cyclic force-time history (Fig. 3) varying from 960 to 480 kN (p32 test) was modeled numerically in 3D to verify and calibrate the developed framework for the dynamic analysis of the model. Lateral loads were applied at 1.6 m above the soil surface, 1 m below the head of the pile model with an embedded length of 12 m in dense sand.

The constitutive soil model parameters were summarized in Table 2. It can be inferred from the literature that, overall, the response observed in a soil element can not be directly transferred to a soil-foundation system owing to the difference between drainage conditions in test and in situ conditions (i.e., generation of 3-D hydraulic gradients), existence of local high excess pore pressures around the pile, and difference in boundary conditions [1].

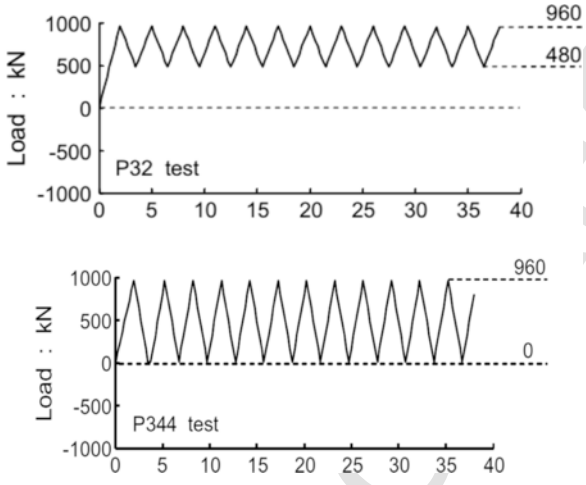

Fig. 3. Load time histories of the tests P32 and P344 [17].

Table 2
Material parameters used for dense sand.

Parameters	Dense sand
Low strain shear modulus, G_r(kPa)	60,000
Friction angle, φ(Degree)	41.8
Liquefaction yield strain, γ_y	1%
Contraction parameter, c_1	0.05
Dilation parameter, d_1	0.8
Dilation parameter, d_2	5
PT angle, φ_{PT}(Degree)	30
Mass density, $\rho\ (kg/m^3)$	1700
Permeability coefficient, k (m/s)	6.6×10^{-5}

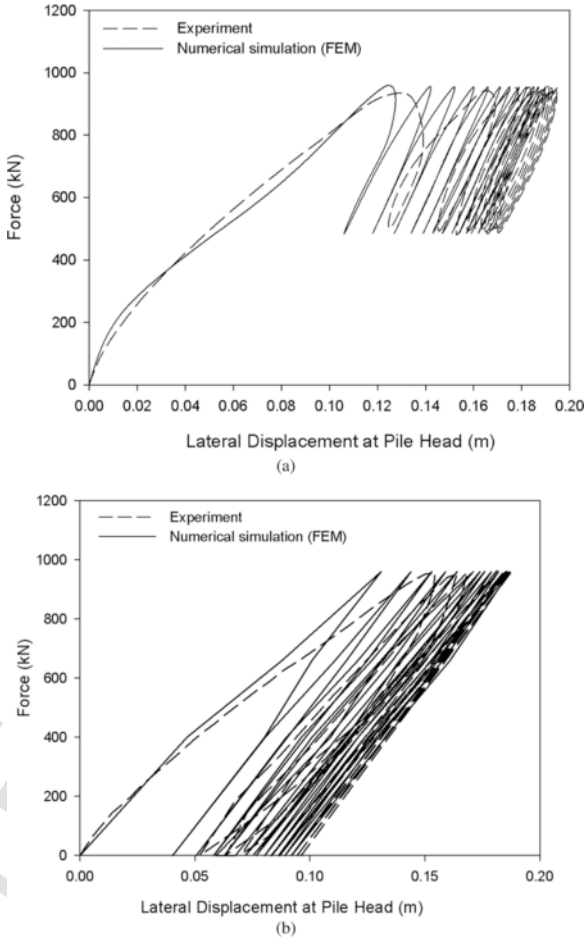

Fig. 4. Experimental and computed force-displacement curves at pile head for tests (a) P32 and (b) P344.

Fig. 4 compares the force-displacement curve of the pile head under the P32 load cycles to the experimental data. Comparison of the numerical predictions for the Soil-Structure Interaction (SSI) with the data measured and computed by [42] indicated that, as expected, the developed model realistically predicted the accumulation of pile displacements in dense sand under cyclic loading.

Rayleigh damping was implemented into the model in which a frequency range of 0.1–5 Hz was set as effective range and 5% Rayleigh damping was assigned to the soil producing the mass and stiffness coefficients as 0.061 and 0.003, respectively.

4. Results and discussion

4.1. Cyclic loading: harmonic excitation

It seems logical to evaluate the behavior of a monopile subjected to cyclic lateral loading through the accumulated rotation rather than the lateral deformation of the pile [43]. Therefore, the main part of this article involves the evolution of rotational deformations. Initially, a series of FE static pushover-type of analyses was performed at different values of moment arm, h to derive the bearing strength envelope of the soil-monopile system (Fig. 5). Also shown on the figure are ranges of ξ_b for $h=30$ m. This parameter is described in subsequent sections modeling the cyclic loading ranges. Fig. 5 interpreted the FE results in terms

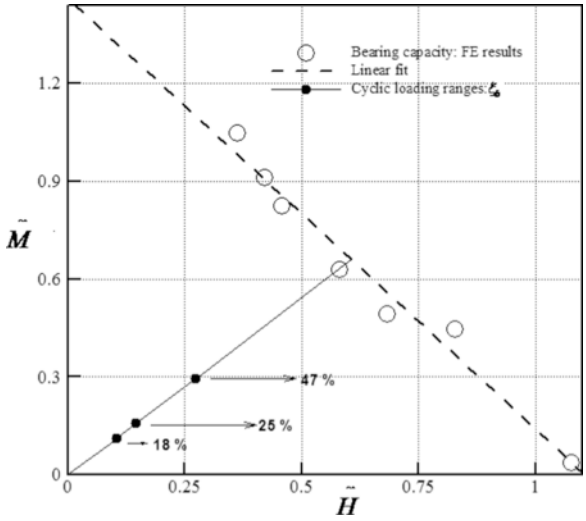

Fig. 5. Failure envelope obtained from bearing capacities obtained at different values of h for large-diameter monopile ($L = 30$ m).

of non-dimensional groups as suggested by [31]:

$$\tilde{M} = \frac{M}{D\gamma L^3}$$
$$\tilde{H} = \frac{H}{D\gamma L^2} \quad (2)$$

In which H and M denote horizontal load and moment at the sea-bed resulting lateral displacement and rotation.

Fig. 6 outlines the evolution of the soil yield computed from the FE analysis and its progressive extension to greater depths in conjunction with load levels. Soil plasticity developed in the vicinity of the monopile head at small strain levels, although only the upper part (i.e., active length) participated in failure.

It was however difficult to identify a failure point from static analyses. A limiting value for the horizontal capacity was defined as ~40 MN which was chosen by taking into account the limiting pile head displacement, 0.1D criterion into account proposed by [10].

Comparisons of the calculated bending moments, shear forces and soil reactions at different stages of virgin loading are presented. The shear force and soil reaction may be calculated indirectly from the bending moment by double differentiation (Fig. 7) at different stages of virgin loading. The model captured the increase in the magnitude of the maximum soil reaction, and the depth at which the maximum occurred.

4.1.1. Cutoff frequency

The developed model, considering homogeneous soil conditions, was subjected to a sinusoidal dynamic load of 10 MN, applied at the top of the monopile. Two vibration periods which are deliberately higher and lower than the first natural period of the soil profile, ($T = 5\ s\ \rangle T_{soil} = 0.45\ s$ and $0.13\ s\ \langle T_{soil} = 0.45\ s$) and two model sizes (50 and 100 m) were investigated. Under a short excitation period (Fig. 8(b)), the lateral boundaries had a clear influence on the response. A large amount of undamped wave energy was present in the model domain. In contrast, the response under the long-period excitation (Fig. 8(a)) was hardly distinguishable between the two model sizes. However, the radiated seismic energy was negligible, providing additional evidence for the existence of a cutoff frequency. Considering the above model verification, to reduce the computational cost in the nonlinear dynamic analysis, a distance of 50 m was adopted in all of the subsequent cases.

4.1.2. Analysis of cyclic rotation

In spite of the existence of the lateral loading for offshore monopiles, four important design loads for offshore monopiles have been described [12,31,54]:

- Ultimate Limit State (ULS), experienced once during the wind turbine lifetime;
- Worst expected transient load (WETL = ULS/1.35), experienced once during the lifetime;
- SLS (~47% of the ULS), experienced frequently (~100 times) during the lifetime; and
- FLS (25–30% of the ULS), experienced very frequently (~10^7 times) during the lifetime.

Cyclic creep, defined as the accumulation of plastic strain in the vicinity of the pile, is accompanied by hardening or softening of the soil. The cyclic stress ratio of the soil elements, which is used to determine the cyclic creep, corresponds to the cyclic load ratio of the whole soil-pile interaction system. It is defined by the ratio of the cyclic load amplitude to the static bearing capacity of the pile. Two different parameters were defined to characterize the cyclic lateral load by Buckingham's hypothesis [44]:

$$\begin{Bmatrix} \xi_b = \frac{M_{\max}}{M_R} \\ \xi_c = \frac{M_{\min}}{M_{\max}} \end{Bmatrix} \quad (3)$$

in which $M_{\max}$ and $M_{\min}$ are the maximum and minimum moment in the load cycle (plotted in Fig. 9), and M_R is the static capacity. The loading type is denoted by the dimensionless parameter ζ_c, which typically ranges from 0 (one-way cyclic loading) to -1 (full two-way cyclic loading). Several long-term cyclic loading analyses were performed, in both saturated and dry sands. Analyses were conducted with one-way cyclic loading and a target $\zeta_c = 0$. The loading magnitudes were chosen to reflect realistic loading conditions for the FLS and SLS. Different load regimes of types A, B, and C are listed in Table 3.

The moment-rotation curves governed by static and cyclic loads are presented in Fig. 10. Dense sand can be expected to show a stiffer re-

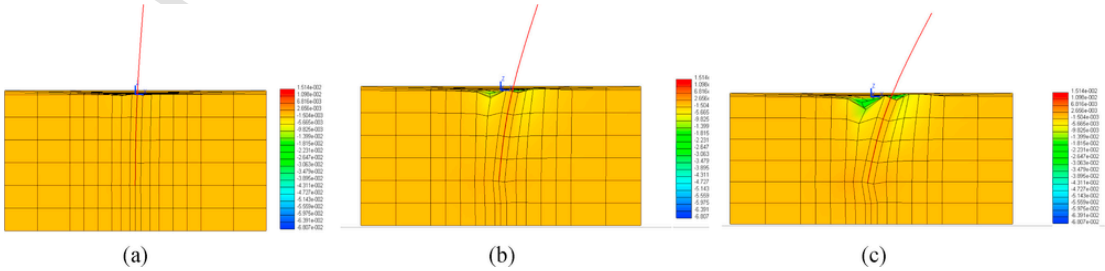

Fig. 6. Contours of plastic strain magnitude (plotted as deformed mesh) at selected loading levels (as a fraction of the total applied load) for a shear force monotonically applied at the head of the monopile (a 57,000 kN shear force monotonically applied at the head of monopile: $h = 30$ m). a) H = 0.175 H_{ult}, b)H = 0.33 H_{ult}, c) H = 0.7 H_{ult}.

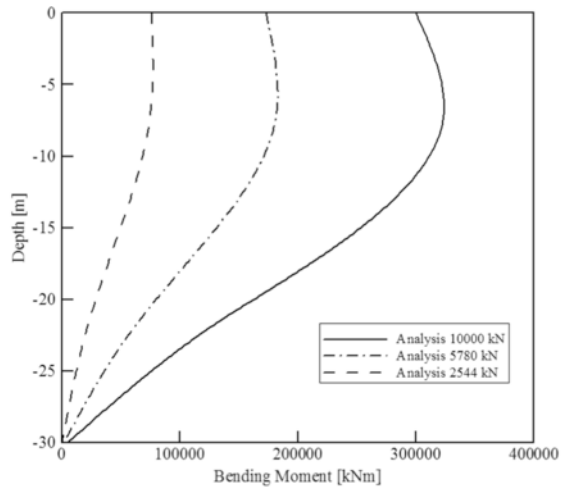

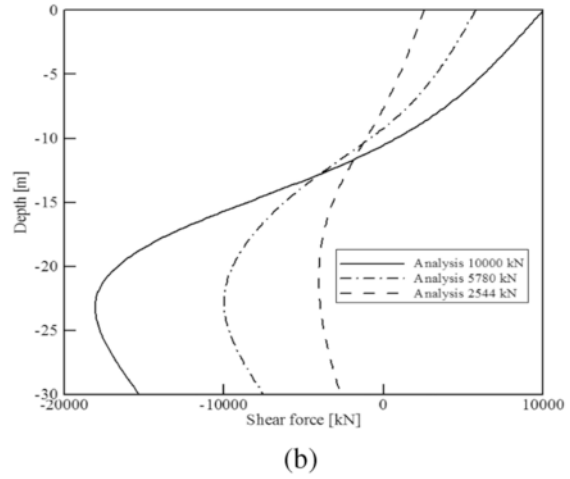

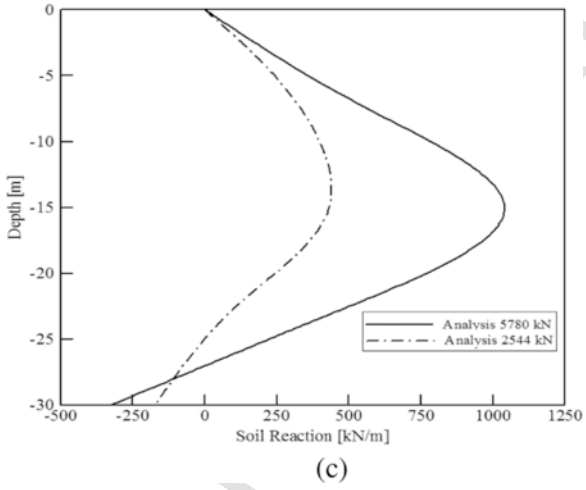

Fig. 7. Computed (a) bending moment b) shear force c) soil reaction distribution for virgin loading of monopile at 10,000 kN, 5780 kN, 2544 kN.

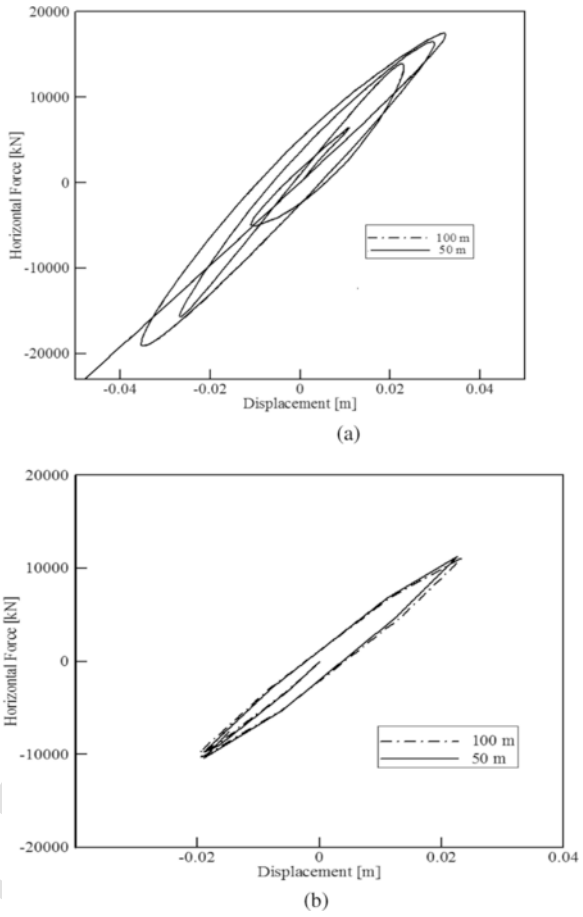

Fig. 8. Model verification: proof of the existence of a cutoff period for radiation damping. Harmonic excitation at the top of the monopile. The response for two vibration periods (a) $T \rangle T_{soil}$, (b) $T \langle T_{soil}$ and two model sizes (FE model length = 50 and 100 m) is analyzed.

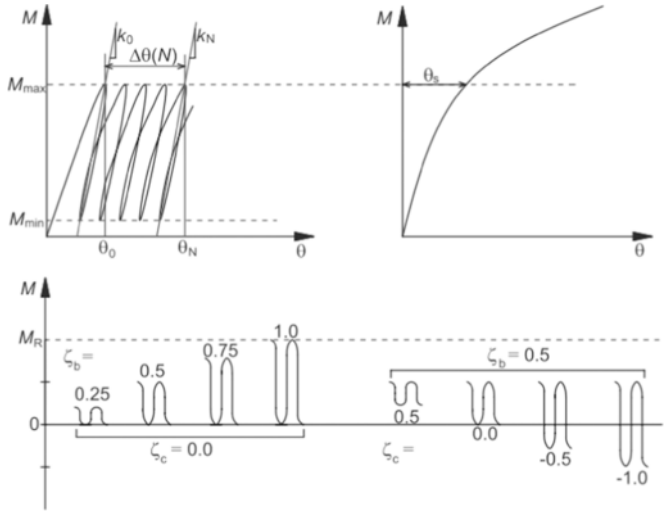

Fig. 9. Cyclic parameters ([44]; LeBlanc et al., 2009).

sponse than its initial state, as previously reported by [43]. The rotation in the first loading cycle was almost equal to the rotation obtained in the static pushover analysis (Fig. 10). The cyclic triaxial tests carried out by [35] indicated that the stress exponent (herein called the load exponent) of the stress-strain curve follows a quadratic relationship. Figs. 11 and 12 present the pile rotation at the soil surface as a function of the number of cycles (N).

According to [44], most functions for the displacement of structures under cyclic loading are either exponential or logarithmic as follows:

Table 3
Loading characteristics.

Load regime	ξ_b	ξ_c	θ_s: rad	θ_1 : rad
A	0.18	0	1.89×10^{-3}	1.45×10^{-3}
B	0.25	0	4.29×10^{-3}	3.24×10^{-3}
C	0.47	0	5.1×10^{-3}	4.65×10^{-3}

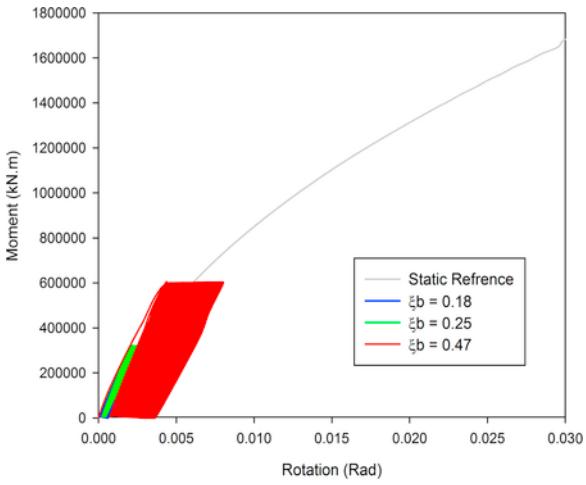

Fig. 10. Moment-rotation relationships of the static reference analysis and the four cyclic loads ($D = 7.5$ m, $L = 30$ m, $h = 30$ m).

$$\left\{ \begin{array}{ll} \frac{\Delta\theta}{\theta_1} = aN^b & (a) \\ \frac{\Delta\theta}{\theta_1} = a + \ln\ (N)^b & (b) \end{array} \right\} \quad (4)$$

where θ_1 is the rotation obtained in the first loading cycle. Two dimensionless constants a and b can be determined empirically from either physical modeling or numerical analyses.

Both expressions were fitted to the maximum values of the rotation computed in the FE simulations. A varied normalization of the rotation is found in the literature by [31]. The proposed normalization of $\frac{\Delta\theta}{\theta s}$ (where θ_s is the rotation occurring in a static analysis when load is equivalent to $(\xi_b \times M_R)$ is only valid when evaluating the maximum rotation. Fig. 11 shows the computed response of the evolution of the pile rotation, θ, at the soil surface as a function of the number of cycles under three types of continuous cyclic loading for dry sand. Rotation accumulated throughout the entire analysis, and similar trends were obtained in two additional analyses for saturated sand (Fig. 12). In these evaluations, the maximum values of the rotation were used (dashed lines in Figs. 11 and 12).

Further inspection of Fig. 10 and Table 3 reveals that $\theta_s \approx \theta_1$; therefore, the accumulated rotations obtained from different cyclic analyses in Fig. 13 were normalised to the rotation obtained in the first loading cycle. Predictions obtained with Eqs. (4a) and (4b) shown in Figs. 13 and 14 suggested that the model well-predicted the accumulated rotation of the stiff pile with a power function, as previously shown by [37]. For dry sand, b ranged from 0.47 to 0.52; these values are larger than the value of $b = 0.31$ reported by [31] for small-scale stiff piles.

Using the data from these simulations, expressions fitting the first 1000 cycles were determined. Similar plots were obtained for saturated sand when the maximum values were fitted. As shown in Table 4, the Pearson correlation coefficients between the computed and fitted expressions were between 0.951 and 0.999, representative of the accumulated rotation of an offshore monopile.

Eq. (4a) can be described more conveniently herein:

$$\frac{\Delta\theta}{\theta_1} = T_b(\xi_b)T_c(\xi_c).N^b \quad (5)$$

where the coefficient a in Eq. (4a) is interpreted by dimensionless functions T_b and T_c in terms of the load characteristics. As such, the function T_c can be assumed here equal to unity, which arises from $\xi_c = 0$.

Hence, on rearranging Eq. (5), the normalised form of accumulated rotation is given by:

$$\frac{\Delta\theta}{\theta_1} = T_b(\xi_b).N^b \quad (6)$$

The results arisen from the assumption of a nearly constant b observed in analyses with respect to the sand saturation (for example $b \sim 0.49$ for dry sand), indicates that T_b depends linearly on the load magnitude, ξ_b, varying in a range between 0.18 and 0.47 (Fig. 15). A similar tendency was observed from small scale tests by [31,44], although the reported values for T_b cover a lower range of variation. However, further studies are required to verify the form of models developed for both dry and saturated sands, and to extend them for predicting long-term behavior of offshore piles.

These findings suggest that lateral cyclic loading on monopiles embedded in cohesionless soils will not typically result in complete shakedown, but instead will result in the progressive accumulation of deformations. [21] called this phenomenon shakedown evolution. In this attenuation mechanism, the rate of displacement will constantly decrease, but will never reach zero, because the effect is modeled in a logarithmic fashion with load cycles. For certain loading cycles, the logarithmic function of the number of cycles (proposed by [21,42 and 32]) is eventually followed by an over-logarithmic accumulation stage for higher numbers of load cycles. The validity of this issue was investigated for the FLS, and deformation accumulation was approximated by power laws in contrast to the logarithmic formulation.

4.2. Influence of load order

Next, variable cyclic load patterns and the validity of Miner's accumulated damage concept for monopile-dense soil systems were investigated. The accumulated rotations for three load patterns were calculated, considering the effect of load sequence based on Miner's damage concept. Fig. 16 shows rotation envelopes from three loading regimes operated with 1000 cycles of type A, 100 cycles of type B, and 10 cycles of type C, respectively and inversely. The resulting accumulated pile rotations differed by $\Delta\theta = 0.33^{\circ}$. Denser sands had a higher sensitivity to the load sequence, as was reported in the cyclic triaxial tests of [48]. However, the dry sand analyses showed some minor scatter in the order of the load applications.

4.3. Strain superposition theory

[47] advocated the strain superposition theory for load cycles with different amplitudes. This theory states that strains accumulate through the strain accumulation curves developed for different load amplitudes while maintaining the strains implemented in previous events. The accumulated rotation for load type A, $\Delta\theta_a$, may alternatively be obtained through the application of $(N_b)_{Equivalent}$ load cycles of type B, through Eq. (7) [31]:

$$\Delta\theta_a = \left(\theta_1 T_b T_c\right)_a \times (N_a)^{\alpha} \quad (7)$$

where $T_b = T_b\left(\zeta_b, R_d\right)$ and $T_c = T_c\left(\zeta_c\right)$ are dimensionless variables, and R_d represents the soil relative density. If N_a cycles of loading type

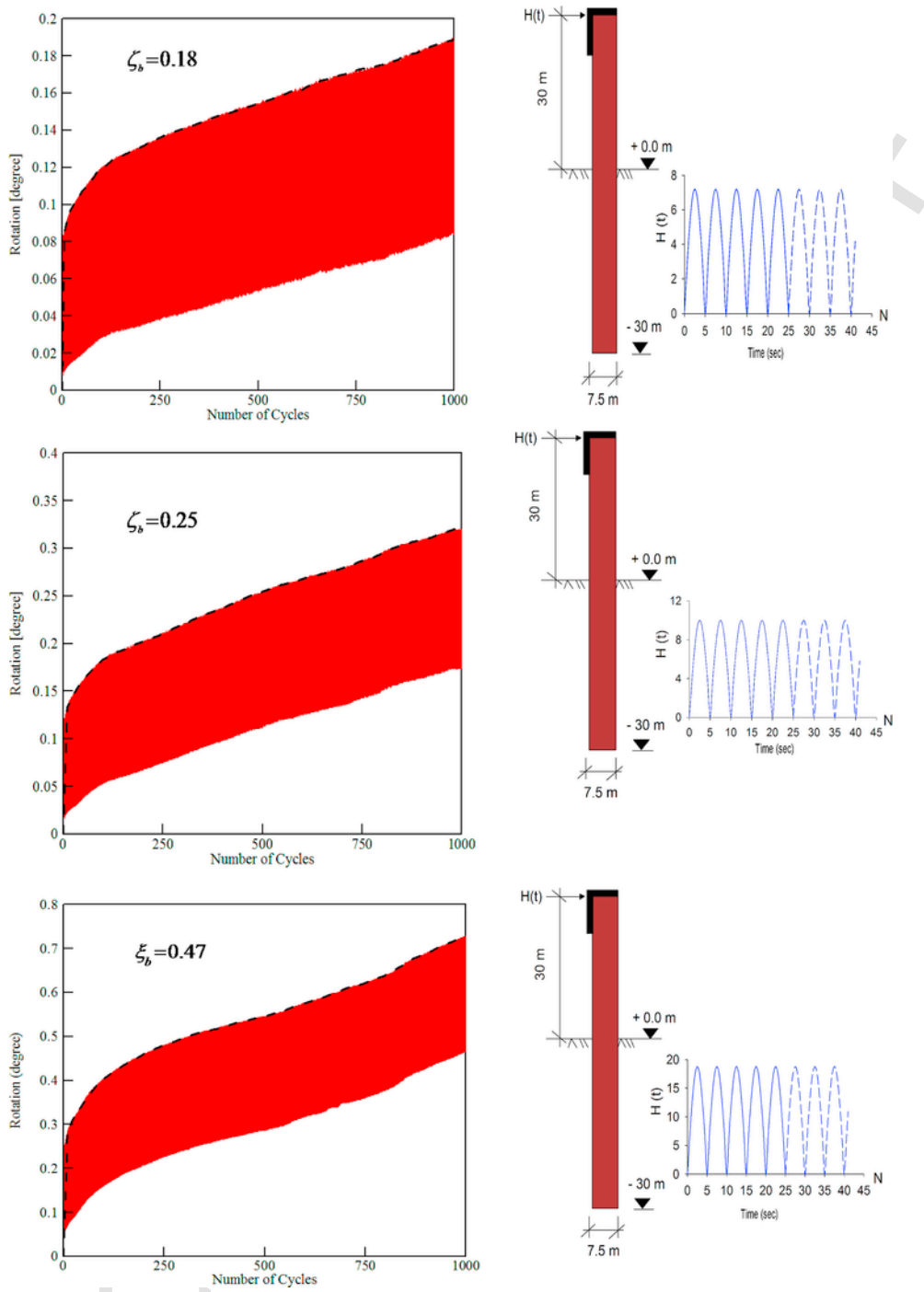

Fig. 11. Rotation of the monopile at soil surface as a function of the number of cycles in the FE simulations with $\xi_b = 0.18,\ 0.25$ and 0.47. Maximum values of rotation are indicated by the dashed lines.

A are applied to the monopile, followed by N_b cycles of loading type B, the resulting rotation may be obtained by [31]:

$$\theta_b = \left(\theta_1 T_b T_c\right)_b \times \left(N_b^{Equivalent} + N_b\right)^{\alpha} + \max\left[\theta_{1,a},\ \theta_{1,b}\right] \quad (8)$$

$$N_b^{Equivalent} = \left(\frac{\Delta\theta_a}{\left(\theta_1 T_b T_c\right)_b}\right)^{1/\alpha} \quad (9)$$

Fig. 17 shows the predicted monopile rotation in response to the load sequence 200A---200B. In general, satisfactory agreement was found between the theoretical solution and computed curves.

4.4. Effect of load reversal

Next, consider load pattern type A, defined by the corresponding ξ_b . Another cyclic load, identified by $-\xi_b$ with equivalent amplitude but in the opposite direction, was considered to analyze the effect of load reversal on the accumulation of rotation in the soil-pile system. Fig. 18 depicts the pile rotation under the loading pattern of

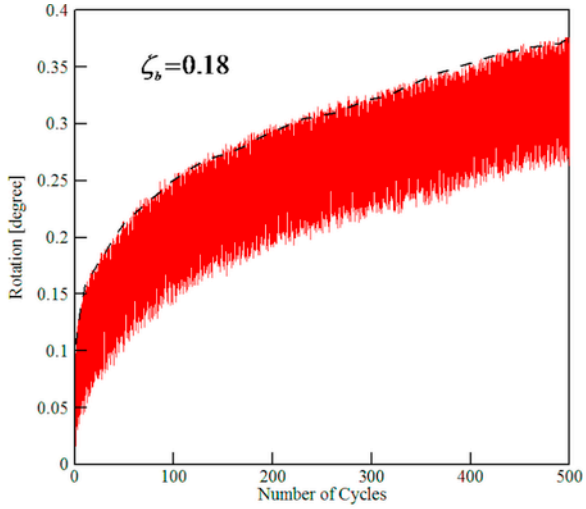

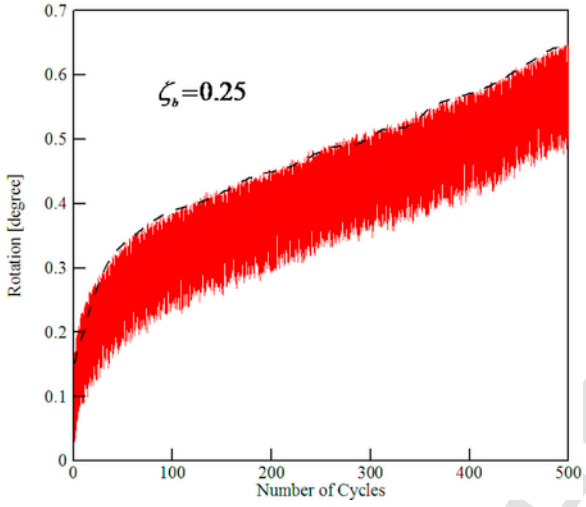

Fig. 12. Rotation of the monopile at soil surface as a function of the number of cycles in the FE simulations with $\xi_b = 0.18$ and 0.25. Maximum values of rotation are indicated by the dashed lines.

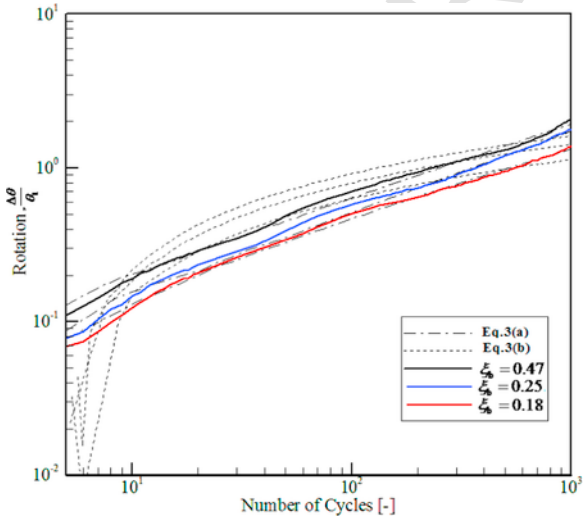

Fig. 13. Normalised accumulated rotation as a function of the number of cycles for the three amplitudes of cyclic loadings for dry sand.

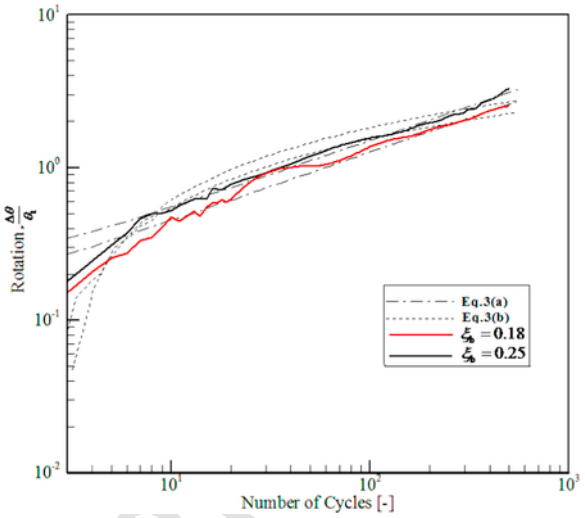

Fig. 14. Normalised accumulated rotation as a function of the number of cycles for the three amplitudes of cyclic loadings for saturated sand.

$(N \times A) \rightarrow (N \times -A) \rightarrow (x \times A)$, where x is the number of cycles needed to diminish the effect of the loading reversal. The accumulated rotation is eventually equal to the rotation prior to load reversal. The results showed that 2.31 N cycles were required to counteract the effects of load reversal on a monopile installed in dense sand, which is higher than the 1.963 N cycles found by [31] for small-scale stiff piles in medium dense sand. Therefore, the hypothesis that 1 N cycles are required to neutralize this phenomenon (i.e., subtraction of the number of reversed load cycles) underestimates the accumulated rotation.

4.5. Fatigue analysis

The model proposed by [32] suggests that the accumulated rotation is proportional to ln(N). This model was investigated in the previous sections for dry sand with $N < 1000$. A relatively good fit was observed, with a better fit when the accumulated rotation was modeled as an exponential rather than a logarithmic expression.

In this section, this issue was further studied for the FLS. The results from fatigue analysis showed a much better fit with the exponential expression ($R = 0.999$) than with the logarithmic expression ($R = 0.851$). Constants a and b for the exponential expression were 0.0324 and 0.58, respectively, and for the logarithmic expression were -2.78, and 0.851, respectively. Table 5 reports the load characteristics for a realistically designed wind turbine, including the FLS, SLS, and the worst expected transient load equal to ULS/1.35. The results include $\sim 10^4$ cycles, whereas FLS is governed by 10^7 load cycles. In the absence of further information, and due to the closeness of the exponential fit up to 10^4 cycles, care should be advised when extrapolating the fitting expression to the FLS.

[31] proposed the following expression based on small-scale tests:

$$\begin{cases} \Delta\theta_i = \left(\left(\Delta\theta_{i-1} \right)^{1/\alpha} + N_i \times \left(\theta_s T_b T_c \right)^{1/\alpha}{}_i \right)^{\alpha} \\ \theta_i = \Delta\theta_i + \max\left(\theta_{s,1}, \ldots, \theta_{s,i} \right) \end{cases} \tag{10}$$

The evolution of pile rotation due to cyclic loading in the above expressions was obtained by employing different assumptions, such as Miner's rule, the strain superposition theory, and the extended rainflow-counting method [45]. For this research, in line with the non-dimensional frameworks given above, the load-time histories are decomposed into a set of load regimes relevant to wind turbines (Table 5).

The maximum accumulated rotation is determined as $\theta_p = 1.917^{\circ}$. Fatigue and serviceability limit states contribute to θ_p by 46% and 20%

Table 4
Pearson's correlation coefficient, R, between the fitted and computed results for the accumulated rotation.

ξ_b (Sand type)	No. of Cycles	Power fit (Eq. (4a))			Logarithmic fit (Eq. (4b))		
		a	b	R	a	b	R
0.18 (Dry)	1000	0.05	0.474	0.998	−0.368	0.217	0.959
0.25 (Dry)	1000	0.045	0.528	0.999	−0.469	0.273	0.951
0.47 (Dry)	1000	0.064	0.492	0.996	−0.493	0.305	0.955
0.18 (Saturated)	500	0.157	0.450	0.997	−0.521	0.445	0.976
0.25 (Saturated)	500	0.185	0.452	0.996	−0.669	0.538	0.964

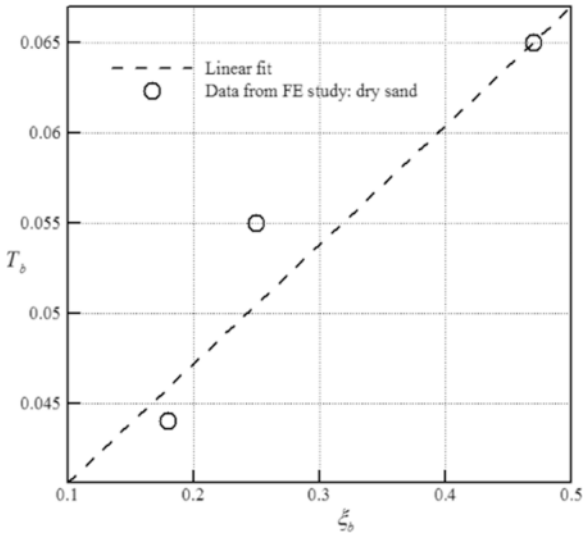

Fig. 15. Fitted empirical constant T_b as a function of the loading magnitude ξ_b in the three cyclic analyses for dry sand.

respectively, rather than 31.82% caused by the worst expected load. From this point, the high-level cycling, even though in very few cycles gave a scope for accelerated accumulation of rotation.

Fig. 19 shows the lateral deflection of two monopiles. The monopile with an embedded length of 30 m behaved like a flexible pile, whereas the short monopile with a length of 20 m showed a rigid response. A significant head-and-toe displacement with increasing load cycles was observed, with a slight downward movement of the rotation point of the pile. Greatest displacement was observed during the first cycle, and the accumulated cyclic displacement increased with the number of cycles.

4.6. Cyclic loading: transient effect

A large-diameter monopile is intended to maintain the serviceability of offshore platforms over several years. However, a monopile with an unfavorable drainage system can lead to the accumulation of PWP, followed by pile displacements. There can be significant changes in the induced loads when waves pass a structure, therefore, transient effects need to be considered.

The PWP pattern changes dramatically with the loading rate, although the loading test frameworks in literature are limited to very poorly drained conditions for small-scale soil-pile models. The change in PWP, Δp, can be defined as follows [10]:

$$\Delta p = f\left(\frac{1}{k}, \frac{1}{T_L}, L_d, \gamma_w\right) \tag{11}$$

where T_L is the loading period, k is the soil permeability, L_d is the drainage length, and γ_w is the unit weight of fluid. Although f is not explicit, it is evident that an increase in monopile size, when T_L and k are

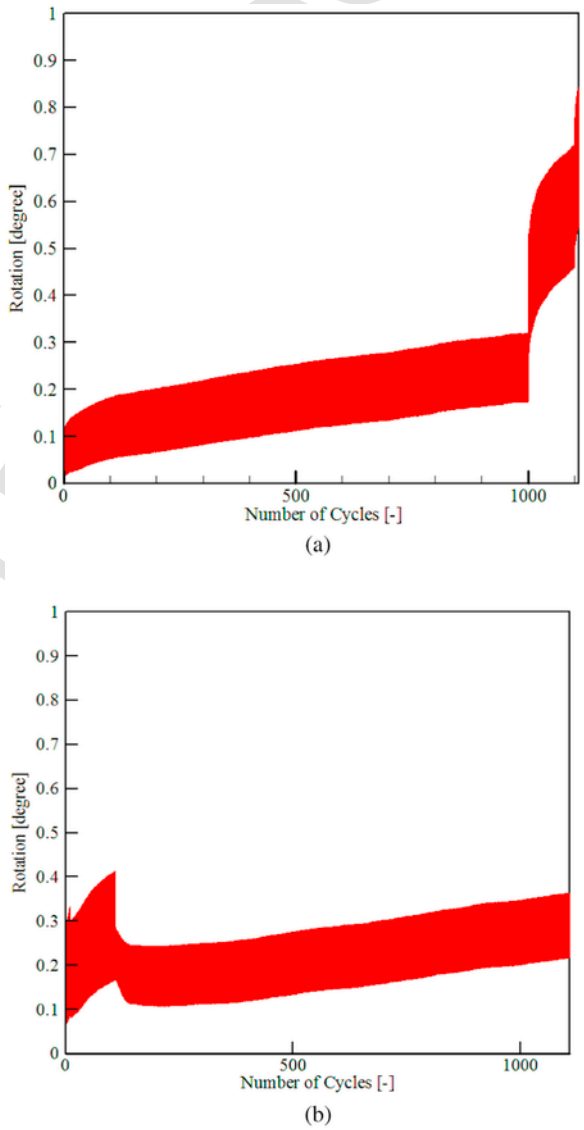

Fig. 16. Envelope of monopile rotation computed for an increasing load sequence. a) 1000A…….100 B…….10C (Dry) b) 10C…….100 B…….1000A (dry).

constant, will lead to greater PWP development. When the period is large, there is very little tendency for PWP development. The developed finite element model was utilized to examine the effects of load repetition, loading rate, and loading history under extreme loading events (Fig. 20(a)). The loading rate had a significant effect on the lateral response of the foundation. Typical responses to such a load history are shown in Fig. 20(b) and (c).

To identify the ground displacement pattern at the soil-pile interface, two cases were defined: the pore fluid behavior in soil adjacent to

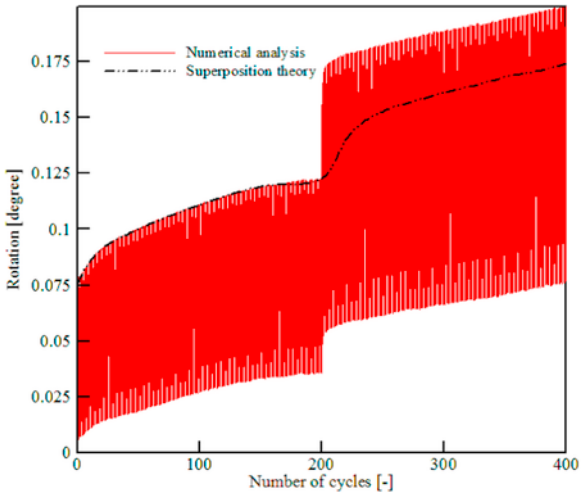

Fig. 17. Prediction of accumulated rotation using superposition concept.

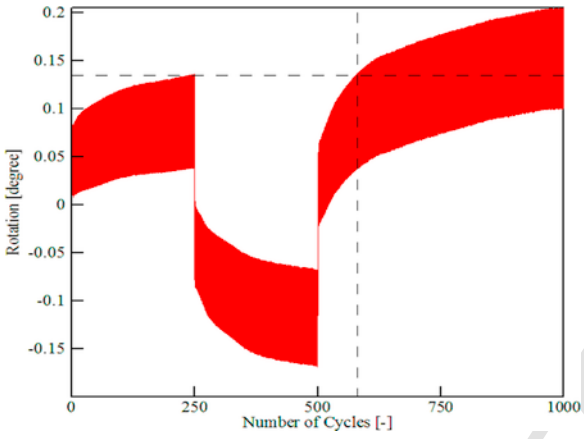

Fig. 18. Effect of the reversed loading on the behavior of monopile rotational deformations: $(\xi_b = 0.18) \rightarrow (\xi_b = -0.18) \rightarrow (\xi_b = 0.18)$.

Table 5
Prediction of the cumulative rotation based on the numerical analysis of a full-scale offshore monopile.

Load type	N	θ_1[degree]	T_b	T_c
FLS	10^7	0.1155	0.0324	1
SLS	100	0.237	0.0648	1
WETL	–	0.61	–	–
Accumulated rotation obtained by Eq. (10)				
Load type	I	$\Delta\theta_i$	$\max(\theta_{1,1},...,\theta_{1,i})$	θ_i
FLS	0	0.783	0.1155	0.89
SLS	1	0.79	0.237	1.027
WETL	2	–	0.61	θ_p = 1.917
Accumulated rotation for continuous cyclic loading obtained by Eq. (4)				
Load type	I	$\Delta\theta = (\theta_1 T_b T_c)_i \times N^{\alpha}$	$\theta = \theta_1 + \Delta\theta$	θ_i
FLS	0	0.783	0.899	46%
SLS	1	0.148	0.385	20%
WETL	2	–	0.61	31.82%

the monopile shaft (case I), and the free-field behavior at a point approximately midway between the pile and the model boundary (case II). The interface exhibits significant displacements because of the complex effects of deviatoric soil deformation (due to SSI-induced cyclic

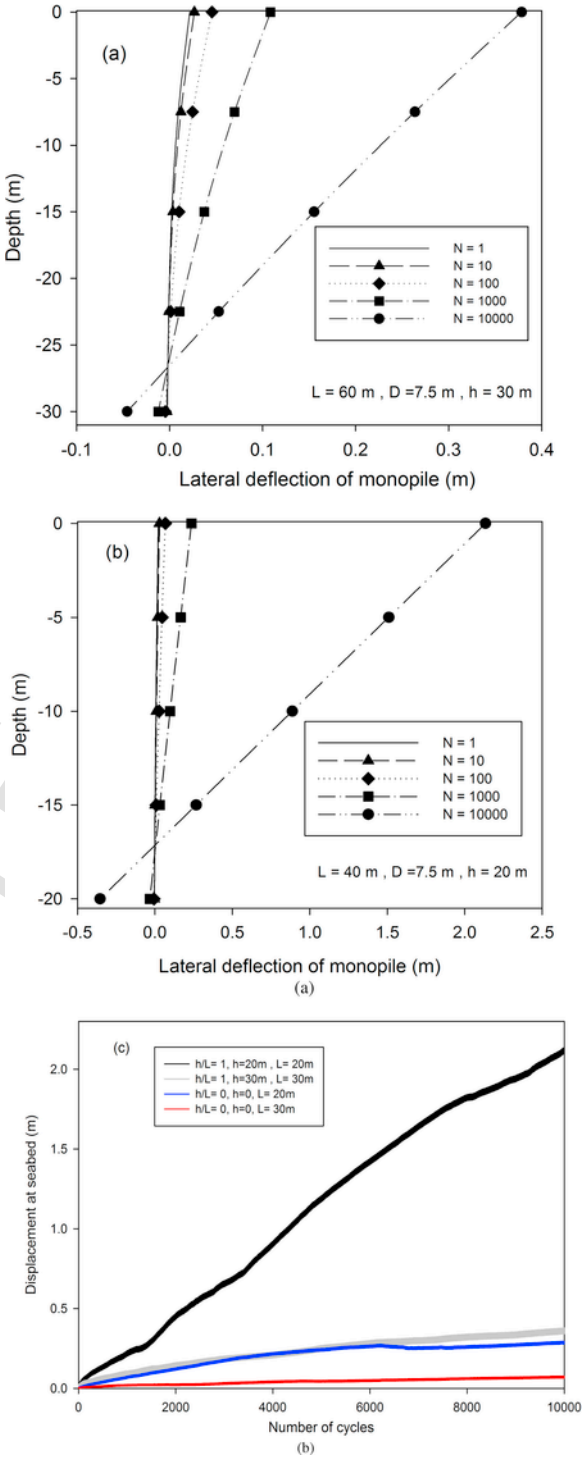

Fig. 19. a) Pile deflection lines under cyclic loading b) Relative increase of the lateral pile displacement at ground level.

loading near the foundation edges) and volumetric effects resulting from dynamic loads. However, there is still insufficient knowledge regarding the mechanisms of foundation-induced dilation in engineering practice, which may lead designers to erroneous decisions.

Under the given level of excitation, a soil compaction mechanism dominated in the free-field, resulting in steadily increasing PWP over ~146 s (Fig. 21(b)). Shear stress components were imposed due to transient excitation, causing the cycle-by-cycle accumulation of lateral

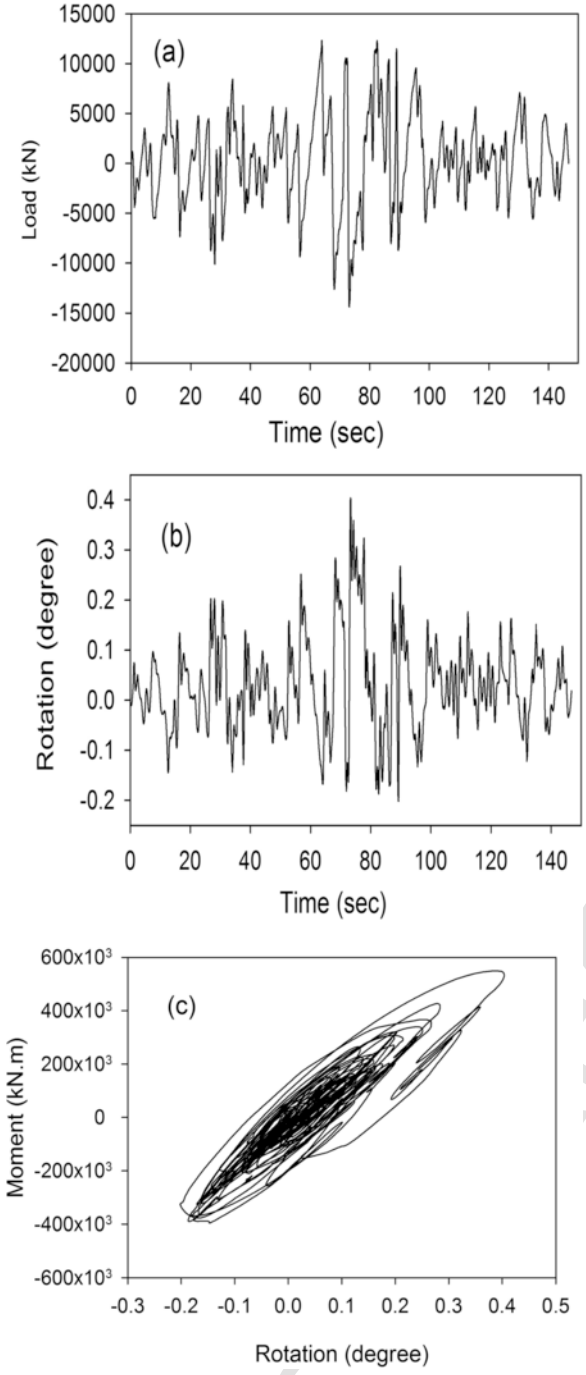

Fig. 20. (a) Loading time history, (b) corresponding displacement response, and (c) the load displacement behavior showing increasing hysteresis for large cycles.

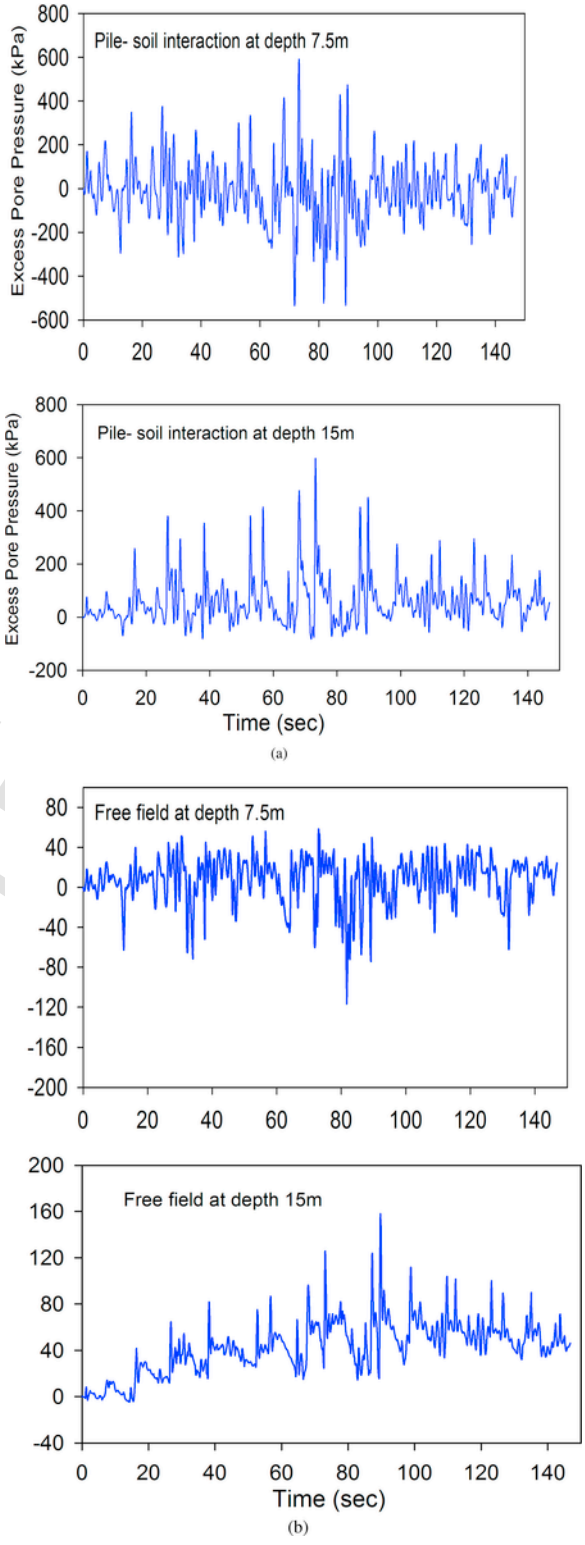

Fig. 21. Representative excess pore water pressure-time histories at various depth. a) soil-pile interface b) interface.

deformations. The computed excess PWP histories (Fig. 21) displayed several instantaneous sharp drops in PWP.

During undrained loading, a zone formed around the pile, in which the PWPs were considerably different from those in the free-field (Figs. 21 and 22). This finding can be attributed to the foundation-induced dilation effect during cyclic loading. Observations from numerical analyses showed that the dilation phenomenon caused by the soil-pile motion on the lateral loading of the monopile head was confined within a zone of approximately up to two diameters in the vicinity of the pile. With the development of 3D transient hydraulic gradients, it is anticipated that partial drainage, PWP, and void redistribution may occur simultaneously. Partial drainage may occur with excess PWP development, in response to transient hydraulic gradients, and as rapidly as the 3D PWP redistribution occurs (Fig. 22). As a result of the horizontal flow towards the free-field, the excess PWP will be dissipated downward.

Shear stress components are imposed by transient effects due to accumulated lateral deformations (Fig. 23). The excess PWP generation

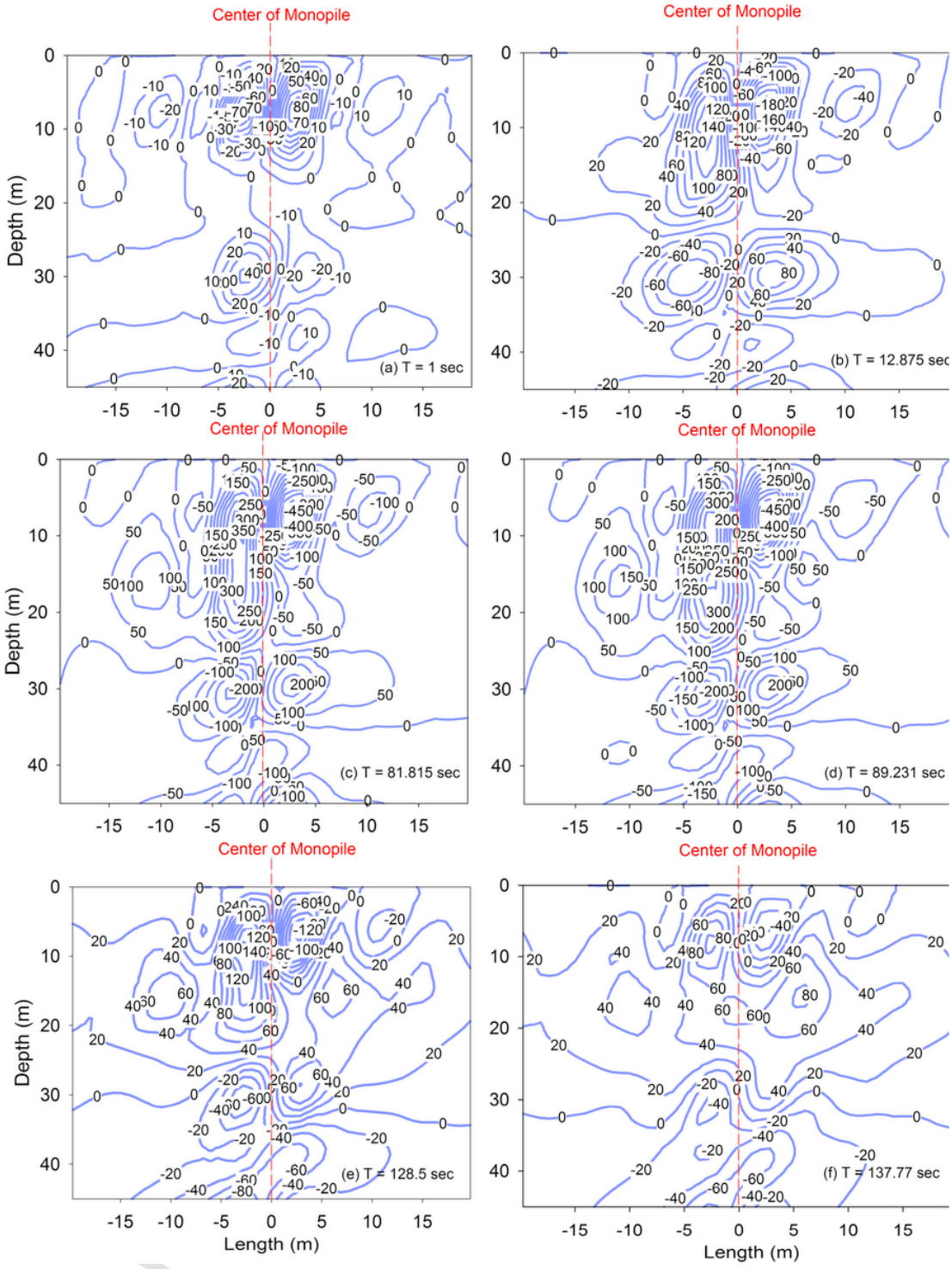

Fig. 22. Three dimensional hydraulic gradients at different instants.

rate and soil softening are highly dependent on the confining pressure and foundation-induced shear stresses.

Storms caused transient and permanent deformations of the foundation and surrounding soil settlements (Fig. 24). The few centimeters of soil settlement indicated that storms, at least of a certain duration, might cause a transient softening of the foundation, until the excess PWP dissipates. Importantly, these a few centimeters pile head deformations were induced in only 146 s. For storms with a return period during the lifetime of a wind turbine, the accumulated deformations may exceed tens of centimeters, which can interrupt the turbine serviceability.

Finally, the SSI-induced settlements were quite similar in shape within the soil layers. The observed re-stiffening behavior towards the end of the motion was mostly due to the vertical downward water flow from the surrounding soil adjacent to the pile shaft toward the free-field (Fig. 22). Settlements in the free-field may be mainly attributed to settlements within the upper layers of saturated sand. Interestingly, the

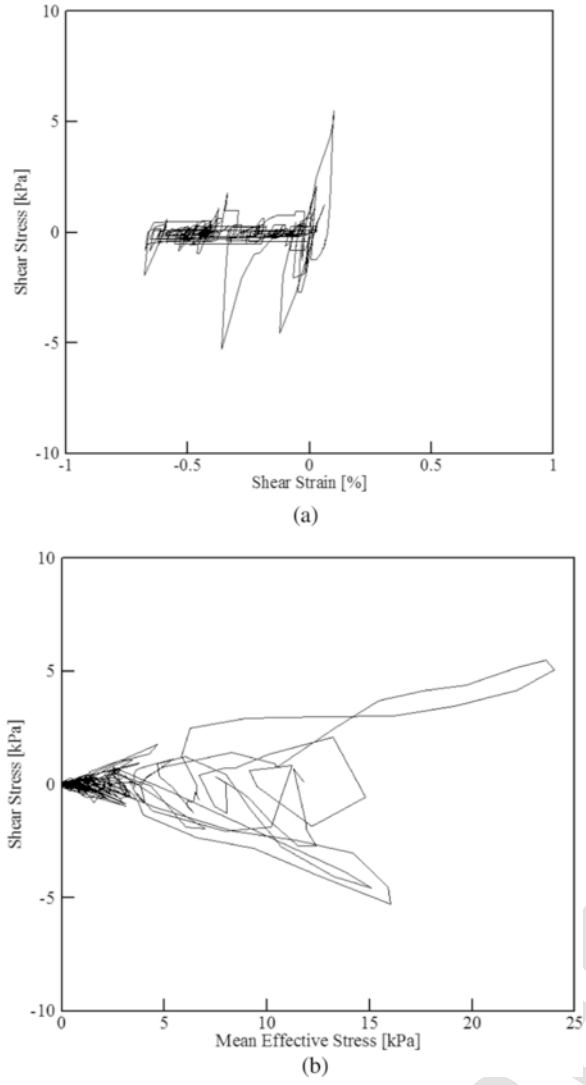

Fig. 23. (a). Computed shear stress histories (b) Computed effective stress path.

downward flow away from the upper layers made late displacements within the lower layers.

5. Conclusions

This paper presents results from the numerical modeling of the lateral long-term cyclic loading of large-diameter monopiles due to wind and tidal waves. A well-calibrated critical state multi-surface plasticity model was employed for modeling the accumulated deformations of offshore piles in dense sand associated with cyclic mobility. This model can be useful for qualitative analysis during the design of foundations for offshore wind turbines, as well as for analyzing how the soil-pile interaction affects the overall response of the system.

Loading conditions corresponded to high lateral loads and bending moments, which could be induced by environmental events, especially storms. When evaluating the cyclic loading, the accumulated rotation was normalised to the rotation obtained in the first loading cycle. For one-way cyclic loading, an attenuation mechanism was observed for different cyclic load ratios, wherein the plastic increments still occurred after a certain number of load cycles and at a decreasing rate to zero, as, for instance, in a logarithmic evolution with the number of cycles. On the other hand, no load level led to an elastic response; therefore, for the dense sand, an attenuating evolution without pure shakedown can generally be expected.

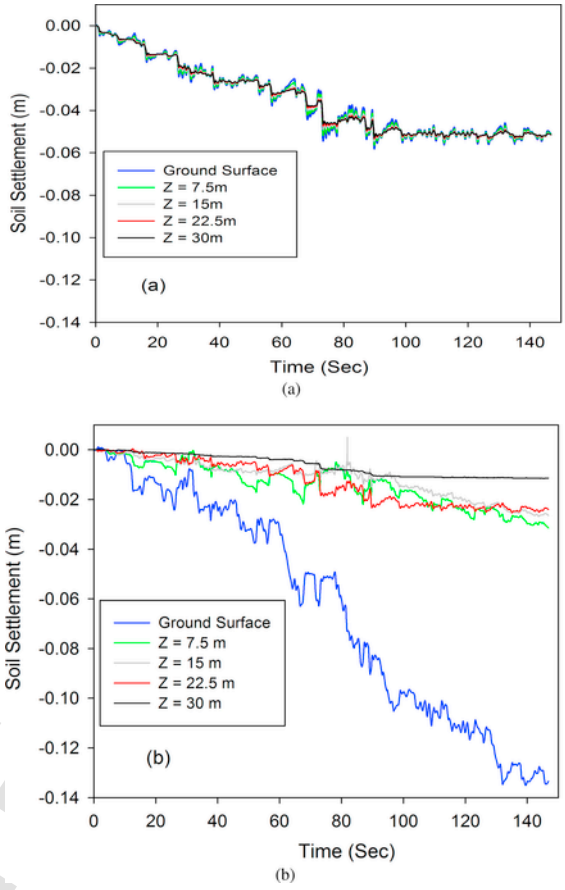

Fig. 24. Settlement-time histories at various depths in the a) soil-pile interface, b) free-field.

The new expressions, which are based on full-scale behavior, are more specific than previously reported relationships because they incorporate additional terms that reflect the soil characteristics during cyclic behavior. Additionally, it was shown that excess PWP may accumulate around the pile, depending on the drainage conditions, system geometry, soil permeability, and load frequency.

Uncited reference

[46].

References

[1] Achmus M, Abdel-Rahman. Design of piles for offshore wind energy foundations with respect to horizontal loading. In: Proceedings of the Twenty-second (2012) International Offshore and Polar Engineering Conference, Rhodes, Greece; 2012.
[2] M. Achmus, Y.S. Kuo, K. Abdel-Rahman, Behavior of monopile foundations under cyclic lateral load, Comput Geotech 36 (2009) 725–735.
[3] American Petroleum Institute (API). Recommended practice for planning, designing and constructing fixed offshore platforms— Working stress design. API Recommended Practice 2A-WSD (RP2A-WSD), 21st Ed., Washington, DC; 2000.
[4] Barari A, Ibsen LB. Effect of embedment on the vertical bearing capacity of Bucket foundations in clay. In: Proceedings 2011 Pan-Am CGS Geotechnical Conference, Toronto, Canada; 2011.
[5] A. Barari, L.B. Ibsen, Undrained response of bucket foundations to moment loading, Appl Ocean Res 36 (2012) 12–21.
[6] A. Barari, L.B. Ibsen, Vertical capacity of bucket foundations in undrained soil, J Civ Eng Manag 20 (1) (2014) 1–12.
[7] A. Barari, M. Bayat, M. Saadati, L.B. Ibsen, L.A. Vabbersgaard, Transient analysis of monopile foundations partially embedded in liquefied soil, Geomech Eng 8 (2) (2015) 257–282.

[8] S. Bhattacharya, J.A. Cox, D. Lombardi, D.M. Wood, Dynamics of offshore wind turbines supported on two foundations, Proc Inst Civ Eng: Geotech Eng 166 (2) (2012) 159–169.
[9] S. Bhattacharya, N. Nikitas, J. Garnsey, N.A. Alexander, J. Cox, Lombardi, D. Muir Wood, D.F.T. Nash, Observed dynamic soil–structure interaction in scale testing of offshore wind turbine foundations, Soil Dyn Earthq Eng 54 (2013) (2013) 47–60.
[10] V.P. Cuéllar, Pile foundations for offshore wind turbines: numerical and experimental investigations on the behaviour under short-term and long-term cyclic loading [Ph.D. thesis], Technical University, Berlin, Germany, 2011.
[11] Choi CH, Jang YE, Lee J, Cho SD. A numerical approach for determination of lateral stiffness considering soil-foundation interaction in offshore wind energy system., EWEA 2012; 2012.
[12] Det Norske Veritas. Offshore standard: design of offshore wind turbine structures. DNV-OS-J101, Hovek, Norway; 2007.
[13] Det Norske Veritas (DNV). Offshore standard DNV-OS-J101 design of offshore windturbine structures. Version October 2007, amended November 2009, Hoevik, Norway; 2009.
[14] Diaz ND, Amat PS. GiD the personal pre/postprocessoruser's manual., Version 5.0, CIMNE, Barcelona, Spain; 1999. ⟨http://gid.cimne.upc.es⟩.
[15] P. Doherty, K. Gavin, Laterally loaded monopile design for offshore wind farms, Proc ICE- Energy 165 (1) (2012) 7–17.
[16] A. Elgamal, Z. Yang, E. Parra, A. Ragheb, Modeling of cyclic mobility in saturated cohesionless soils, Int J Plast 19 (2003) 883–905.
[17] S. Giannakos, N. Gerolymos, G. Gazetas, Cyclic lateral response of piles in dry sand: finite element modeling and validation, Comput Geotech 44 (2012) 116–131.
[18] A. Gotschol, Veränderlich elastisches und plastisches Verhalten nichtbindiger Böden und Schotter unter zyklisch-dynamischer Beanspruchung [Ph.D. thesis], Universität Kassel, 2002.
[19] Haigh SK. Foundations for offshore wind turbines. In: Proceedings of the 8th International Conference on Physical Modelling in Geotechnics, ICPMG 2014. Vol. 1; 2014, p. 153–9; .
[20] He L. Liquefaction-induced lateral spreading and its effects on pile foundations. [Ph.D. thesis], University of California San Diego; 2005, 402 p.
[21] Hettler A. Verschiebungen starrer und elastischer Gründungskörper in Sand bei monotoner und zyklischer Belastung. Veröffentlichungen des Instituts für Bodenmechanik und Felsmechanik der Universität Fridericiana in Karlsruhe, Heft. Vol. 90; 1981.
[22] L.B. Ibsen, A. Barari, K.A. Larsen, An adaptive plasticity model for bucket foundations, J Eng Mech, ASCE 140 (2) (2014) 361–373.
[23] L.B. Ibsen, K.A. Larsen, A. Barari, Calibration of failure criteria for Bucket foundations under general loading, J Geotech Geoenviron Eng, ASCE (2014) http://dx.doi.org/10.1061/(ASCE)GT.1943-5606.0000995.
[24] L.B. Ibsen, A. Barari, K.A. Larsen, Effect of embedment on the plastic behavior of bucket foundations, J Waterw, Port, Coast, Ocean Eng, ASCE (2015) http://dx.doi.org/10.1061/(ASCE)WW.1943-5460.0000284.
[25] K. Ishihara, F. Tatsuoka, S. Yasuda, Undrained deformation and liquefaction of sand under cyclic stresses, Soils Found 15 (1) (1975) 29–44.
[26] Klinkvort RT, Leth CT, Hededal O. Centrifuge modelling of monopiles in dense sand at The Technical University of Denmark. In: Proceedings of the 2nd European conference on Physical Modelling in Geotechnics, Eurofuge.; 2012.
[27] Y.S. Kuo, M. Achmus, K. Abdel-Rahman, Minimum embedded length of cyclic horizontally loaded monopiles, J Geotech Geoenviron Eng 138 (3) (2012) 357–363.
[28] Kirkwood PB, Haigh SK. Centrifuge testing of monopiles subject to cyclic lateral loading. In: Proceedings of the 8th International Conference on Physical Modelling in Geotechnics 2014 (ICPMG2014), Perth, Australia; 2014, p 827–31.
[29] K.A. Larsen, L.B. Ibsen, A. Barari, Modified expression for the failure criterion of bucket foundations subjected to combined loading, Can Geotech J 50 (12) (2013) 1250–1259.
[30] C. LeBlanc, Design of offshore wind turbine support structures - selected topics in the field of geotechnical engineering [Ph.D. thesis], Aalborg University, 2009.
[31] C. LeBlanc, G. Houlsby, B. Byrne, Response of stiff piles to long-term cyclic lateral load, Geotechnique 60 (2) (2010) 79–90.
[32] S.-S. Lin, J.-C. Liao, Permanent strains of piles in sand due to cyclic lateral loads, ASCE J Geotech Geoenviron Eng 125 (9) (1999) 798–802.
[33] D. Lombardi, S. Bhattacharya, D.M. Wood, Dynamic soil–structure interaction of monopile supported wind turbines in cohesive soil, Soil Dyn Earthq Eng 49 (2013) 165–180.
[34] S. Mazzoni, F. McKenna, G.L. Fenves, Open system for earthquake engineering simulation user manual, Pacific Earthquake Engineering Research Center, University of California, Berkeley, 2010. http://OpenSees.berkeley.edu/.
[35] A. Niemunis, T. Wichtmann, T. Triantafyllidis, A high-cycle accumulation model for sand, Comput Geotech 32 (4) (2005) 245–263.
[36] O'Neill MW, Murchison JM, An evaluation of p-y relationships in sands, Research Report No. GT-DF02-83, University of Houston, Department of Civil Engineering; 1983.
[37] Peralta P, Achmus M. An experimental investigation of piles in sand subjected to lateral cyclic loads. In: Proceedings of the 7th International Conference on Physical Modeling in Geotechnics, Zurich, Switzerland; 2010.
[38] J.H. Prevost, A simple plasticity theory for frictional cohesionless soils, Soil Dyn Earthq Eng 4 (1) (1985) 9–17.
[39] Qin H, Guo WD. An experimental study on cyclic loading of piles in sand. In: Proceedings of the 10th Australia new Zealand Conference on Geomechanics, Carillon Conference Management; 2007.
[40] F. Rackwitz, S. Savidis, E. Taşan, New design approach for large diameter offshore monopiles based on physical and numerical modelling, GeoCongress 2012 (2012) 356–365.
[41] Reese LC, Cox WR, Koop FD. Analysis of laterally loaded piles in sand, In: Proceedings of the Sixth Annual Offshore Technology Conference, Houston, Texas. paper no. OTC 2080; 1974.
[42] Rosquoet F, Garnier J, Thorel L, Canepa Y. Horizontal cyclic loading of piles installed in sand: study of the pile head displacement and maximum bending moment. Triantafyllidis T, editor. In: Proceedings of the International Conference on Cyclic Behaviour of Soils and Liquefaction Phenomena, Bochum: Taylor & Francis; 2004, p. 363–8.
[43] Roesen HR, Andersen LV, Ibsen LB, Foglia A. Experimental setup for cyclic lateral loading of Monopiles in sand. In: Proceedings of the International Ocean and Polar Engineering Conference, Rhodes, Greece; 2012.
[44] Roesen HR, Ibsen LB, Andersen LV. Experimental testing of monopiles in sand subjected to one-way long-term cyclic lateral loading. In: Proceedings of the 18th International Conference on Soil Mechanics and Geotechnical Engineering, Paris; 2013.
[45] I. Rychlik, A new definition of the rainflow cycle counting method, Int J Fatigue 9 (2) (1987) 119–121.
[46] Statoil, Hywind Scotland pilot park project EIA scoping report, Xodus Group Ltd, Edinburgh, 2013.
[47] H.E. Stewart, Permanent strains from cyclic variable-amplitude loadings, J Geotech Eng 112 (6) (1986) 646–660.
[48] Shen C, Harder L, Vrymoed J, Bennet W. Dynamic response of a sand under random loadings. In: Proceedings of ASCE Speciality Conference on Earthquake Engineering and Soil Dynamics; 1978, p. 853–63.
[49] H.E. Tasan, F. Rackwitz, S.A. Savidis, Behaviour of cyclic laterally loaded large diameter monopiles in saturated sand, Proc Numer Methods Geotech Eng (2010) 889–894.
[50] Wichtmann T, Niemunis A, Triantafyllidis T. Prediction of long-term deformations for monopile foundations of offshore wind power plants. In: Proceedings of the 11th Baltic Sea Geotechnical Conference: Geotechnics in Maritime Engineering, Gdansk, Poland; 2008.
[51] T. Wichtmann, Explicit accumulation model for non-cohesive soils under cyclic loading [Ph.D. thesis], Fakultät für Bauingenieurwesen der Ruhr-Universität Bochum, 2005.
[52] Z. Yang, A. Elgamal, E. Parra, A computational model for cyclic mobility and associated shear deformation, J Geotech Geoenviron Eng 129 (12) (2003) 1119–1127.
[53] Z. Yang, A. Elgamal, Influence of permeability on liquefaction-induced shear deformation, J Eng Mech 128 (7) (2002) 720–729.
[54] B. Zhu, B.W. Byrne, G.T. Houlsby, Long-term lateral cyclic response of suction caisson foundations in sand, J Geotech Geoenviron Eng, ASCE 139 (1) (2013) 73–83.